Supplemental Information

Cholesterol Depletion by MβCD Enhances Cell Membrane Tension and Its Variations-Reducing Integrity

Arikta Biswas, Purba Kashyap, Sanchari Datta, Titas Sengupta, and Bidisha Sinha

Table S1

Calculation of spatio-temporal parameters of membrane fluctuations			
Parameters	**Description**	**Types of averaging**	**Used in figures**
Mean relative height	Relative height of the membrane in a single pixel, calculated over 2048 frames	Averaged over 144 pixels to give one number per FBR	Figs. S1c, S3c, S5d
		Averaged over all FBRs to give one number per cell	Figs. S1b, S3b, S5c
SD_{time}	RMS value of temporal fluctuations in a single pixel, calculated over 2048 frames	Averaged over 144 pixels to give one number per FBR	Figs. S1c, S3c, S5d
		Averaged over all FBRs to give one number per cell	Figs. S1b, 3d, S5c
$SD(SD_{time})$	Intra-FBR variation of single-pixel RMS of temporal fluctuations, calculated over 2048 frames	Computed from 144 pixels to give one number per FBR	Figs. S1c, S6a
		Averaged over all FBRs to give one number per cell	Figs. 4a, S6a
SD SD_{time}	Intracellular heterogeneity in SD_{time}	SD calculated after clubbing SD_{time} values of all FBRs in a cell to give one number per cell	Fig. 4d
Dissimilar pairs	Intracellular variation of single-pixel RMS of temporal fluctuations	Computed from all FBRs to give one number per cell	Figs. 4b, S6b
SD_{space}	RMS value of spatial height variation in a 2.16x2.16 μm^2 region	Averaged in 20 frames to give one number per FBR	Figs. 2c, S3d, S5d
		Averaged over all FBRs to give one number per cell	Figs. 2d, S3d, S5c
SD SD_{space}	Intracellular heterogeneity in SD_{space}	SD calculated after clubbing SD_{space} values of all FBRs in a cell to give one number per cell	Fig. 4d
λ	Correlation length obtained in a 6.3x1.8 μm^2 region from fitting spatial ACFs to 3-term exponential function	Averaged over 200 frames to give one number per region	Figs. 2c, S5d
		Averaged over all regions to give one number per cell	Figs. 2d, S5c
τ	Correlation time obtained in a pixel by fitting	Averaged in a 0.36x0.36 μm^2 region to give one number per region	Fig. 3a

	temporal ACFs to 3-term exponential function	Averaged in a 2.16x2.16 μm^2 region to give one number per region	Fig. 3a inset
PSD	Power spectrum of temporal fluctuations	Averaged over 144 pixels to get one PSD per FBR	Figs. 2a, S3a, S5b
Parameters extracted from PSD			
Parameters	**Description**	**Types of averaging**	**Used in figures**
$\overline{\sigma(f_1, f_2)}$	Amplitude of temporal fluctuations in a frequency regime	Computed from a PSD to get one number per FBR	Figs. S1c, S3c, S5d
		Averaged over all FBRs to get one number per cell	Figs. 2a, S3b, S5c
Exponent	Frequency dependent power law of the PSD	Computed from a PSD to get one number per FBR	Figs. S1c, S3c, S5d
		Averaged over all FBRs to get one number per cell	Figs. 2a, S3b, S5c
Parameters extracted by fitting PSD			
Parameters	**Description**	**Types of averaging**	**Used in figures**
A	Active temperature	Computed from a PSD to get one number per FBR	Figs. S1e, S3f, S6d
		Averaged over all FBRs to get one number per cell	Figs. 2e, S3e, S6c
η_{eff}	Effective cytoplasmic viscosity	Computed from a PSD to get one number per FBR	Figs. S1e, S3f, S6d
		Averaged over all FBRs to get one number per cell	Figs. 2e, S3f, S6c
γ	Confinement of the membrane	Computed from a PSD to get one number per FBR	Figs. S1e, S3f, S6d
		Averaged over all FBRs to get one number per cell	Figs. 2e, S3e, S6c
σ	Membrane tension	Computed from a PSD to get one number per FBR	Figs. S1e, 3d, S6d
		Averaged over all FBRs to get one number per cell	Figs. 2e, 3d, S6c

Table S1: Calculation of spatio-temporal parameters of fluctuations and mechanical parameters.

Table S2

Parameters	Notation	Values in reports	References	Values calculated in this study
Active temperature	A	3	(1)	3.6±1.1
Effective cytoplasmic viscosity	η_{eff}	2-4*10^4 Pa.s	(2–4)	4162±2010 Pa.s
Bending rigidity	κ	10-50 k$_B$T	(5–7)	Kept constant at 15 k$_B$T (8)
Confinement	γ	2.3*10^8 N/m3, 1.7*105 J/m4	(7, 9)	8.9±4.2x10^8 N/m^3
Membrane tension	σ	3.31*10^{-5} N/m, 10-100 pN/μm, 22-276 pN/μm	(6, 10–12)	565±330 pN/μm

Table S2: Description of the model which is used to extract mechanical parameters.

Figure S1
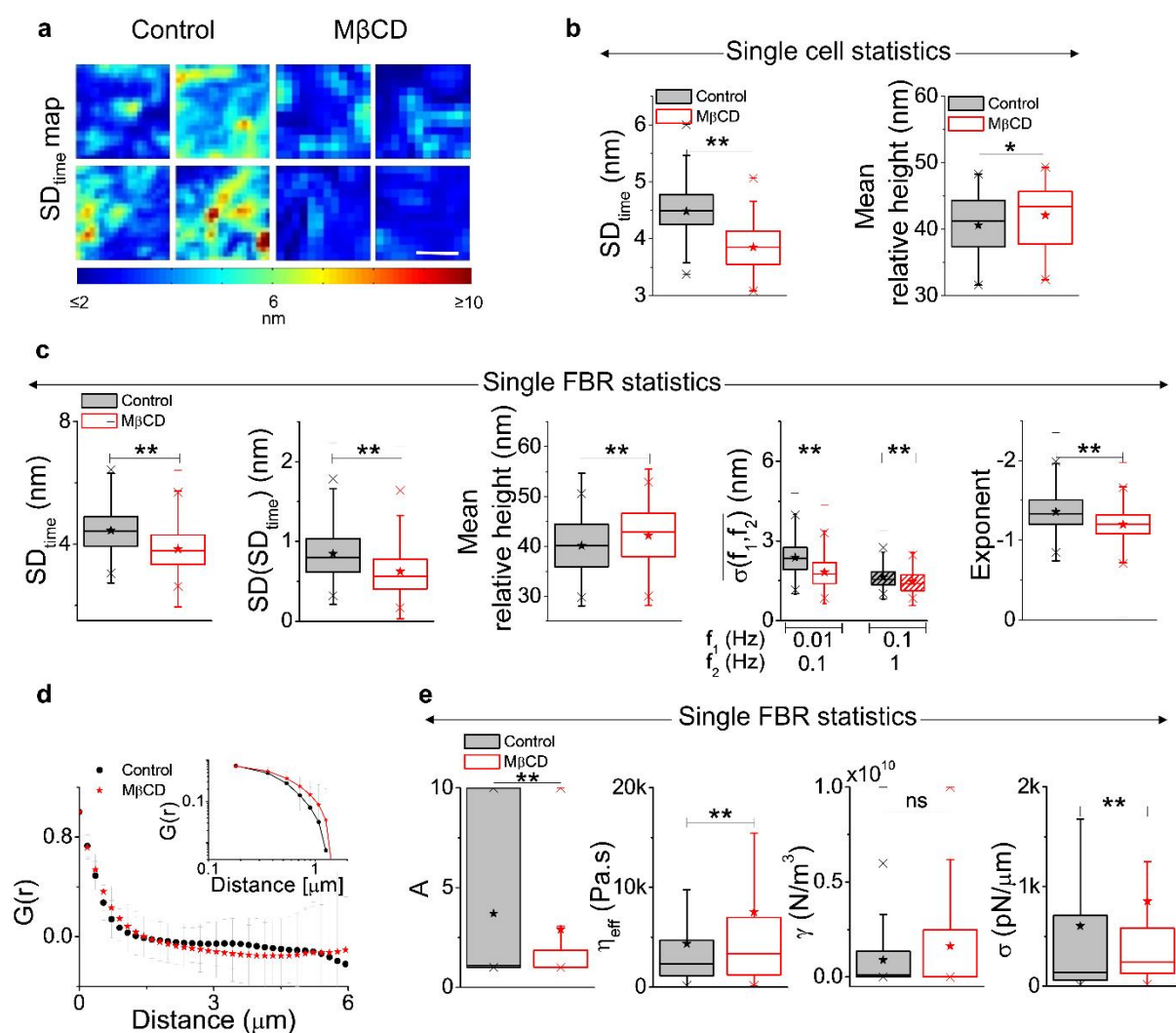
Figure S1: Effect of MβCD on detailed parameters of membrane fluctuations. (a) SD$_{time}$ maps of representative FBRs in control and MβCD treated cells (scale bar: 1 μm). (b) Box plots of SD$_{time}$ and mean relative height in the two conditions. N = 70 cells each. (c) Single FBR statistics of parameters of temporal fluctuations in the two conditions. $n_{control}$ = 1683 FBRs, $n_{MβCD}$ = 1471 FBRs, N = 70 cells each. (d) Averaged spatial ACFs (and their log-log plots, top inset) for control and cholesterol depleted cells. (e) Single FBR statistics of mechanical parameters in control vs. cholesterol depleted cells. $n_{control}$ = 1500 FBRs, $n_{MβCD}$ = 1317 FBRs, N = 70 cells each. * p value < 0.05, ** p value < 0.001, ns p value > 0.05, Mann-Whitney U test. See **Table S4** for statistics.
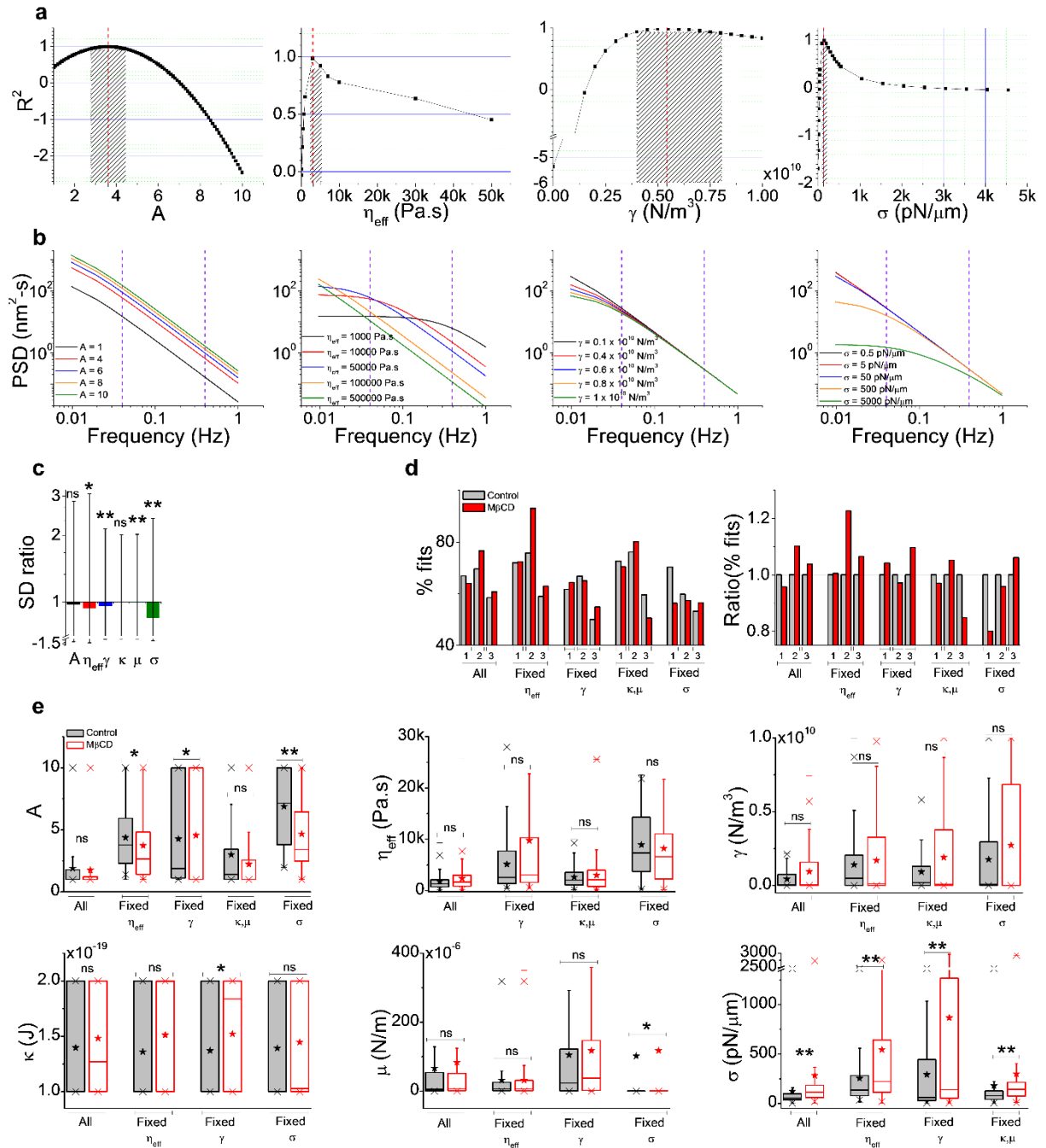
Figure S2

Figure S2: Alterations in membrane tension primarily rule the change in fluctuations. (a) Plots of calculated R^2 with different values of A, η_{eff}, γ, σ to check the sensitivity of the extracted mechanical parameters. (b) Simulations of PSD $PSD(f) = \frac{4\eta_{eff}Ak_BT}{\pi}\int_{q_{min}}^{q_{max}}\frac{dq}{(4\eta_{eff}(2\pi f))^2+\left[\kappa q^3+\sigma q+\frac{\gamma}{q}\right]^2}$ with changing values of A, η_{eff}, γ, σ from low to high numbers to check the robustness of the parameters. The basic power spectrum was constructed with these parameters: A = 1.8083, η_{eff} = 3838 Pa.s, γ = 0.16 x 1010 N/m3, κ = 0.6 x 10-19 J, σ = 74.8 pN/µm. The dashed vertical lines show the regime where the exponent is calculated. (c) Average values of SD ratio simulated from using one-ON approach in MβCD treated (left,

n = 616 simulations) cells of all six parameters. Error bars represent the standard deviation values in each. PSDs $PSD(f) = \frac{4\eta_{eff}Ak_BT}{\pi} \int_{q_{min}}^{q_{max}} \frac{dq}{(4\eta_{eff}(2\pi f))^2 + \left[\kappa q^3 + \frac{9k_BT}{16\pi\kappa}\mu q + \sigma q + \frac{\gamma}{q}\right]^2}$ are simulated from different sets of observed fitting parameters. A whole set of fitting parameters corresponding to a control set are chosen and then only one parameter is changed at a time to that of a MβCD treated set. This is done for each of the parameters – A to σ. The ratio of the SD of the original control set and the SD calculated from the simulated PSD is calculated and the log of these values are plotted to understand the different contributions. Statistics is by students' t-test. (d) Left: plot of % fits in all categories mentioned below in three sets of experiments under control and MβCD treated conditions. $\%\,fits = \frac{No.of\,FBRs\,that\,fit\,to\,the\,model\,in\,the\,mentioned\,category}{Total\,no.of\,FBRs\,analyzed}$. Right: plot of ratio (% fits) between control and MβCD treated cells in the same criteria across three sets of experiments. $Ratio\,(\%\,fits) = \frac{\%\,fits\,in\,M\beta CD\,sets}{\%\,fits\,in\,control\,treated\,sets}$. n = 10 cells each. (e) Mechanical parameters extracted from fitting the PSDs to the theoretical model with minor modifications of control and cholesterol depleted cells. All: none of the parameters are fixed, Fixed η_{eff}: η_{eff} = 3421.27 Pa.s, Fixed γ: γ = 0.08x10^{10} N/m^3, Fixed κ, μ: κ = 1.38x10^{-19} J & μ = 90x10^{-6} N/m, Fixed σ : σ = 368 pN/μm. N = 10 cells, $n_{control}$ = 188 total FBRs, $n_{M\beta CD}$ = 186 total FBRs. * p value < 0.05, ** p value < 0.001, Mann-Whitney U test. See **Table S4** for statistics.
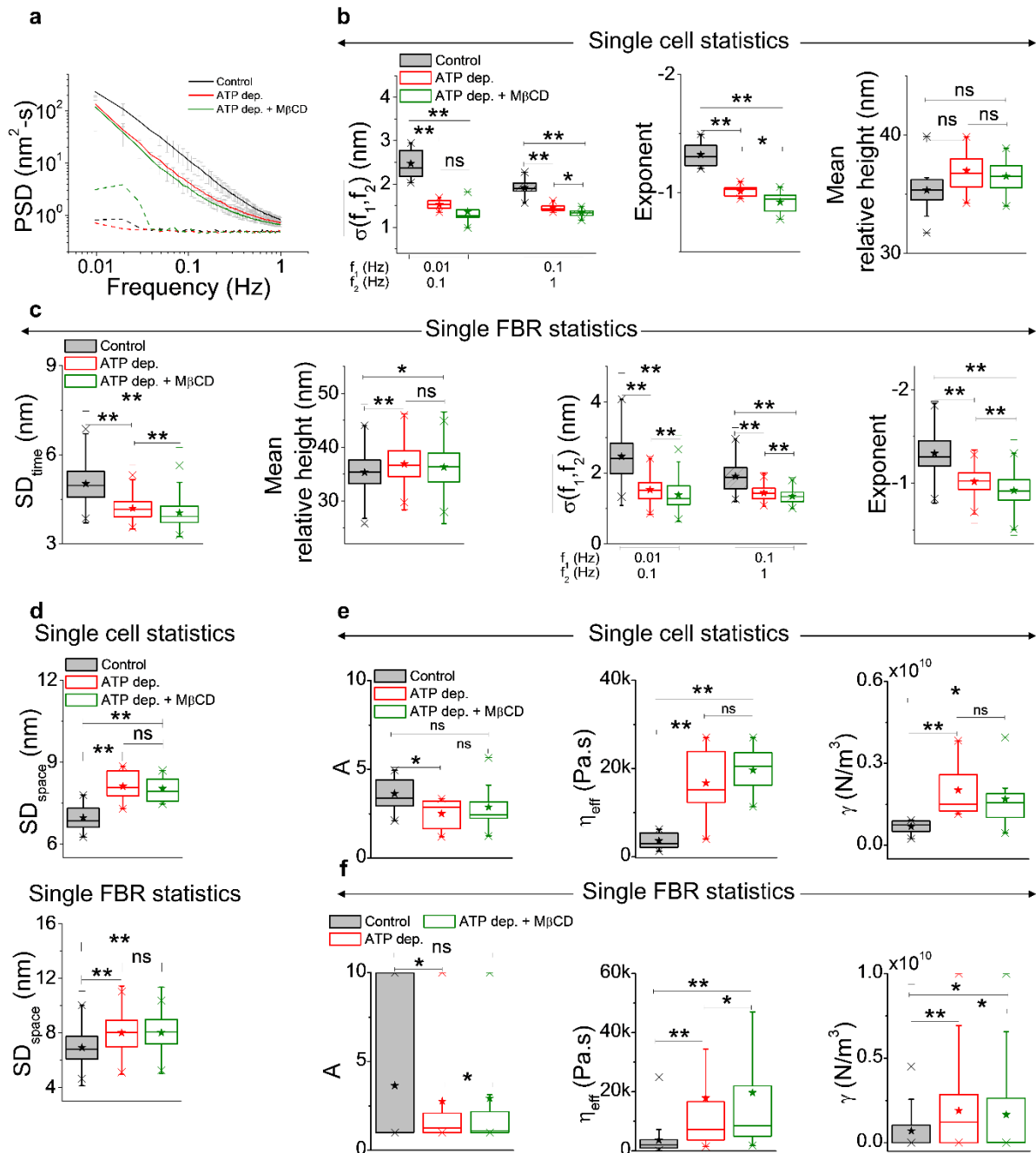
Figure S3

Figure S3: Effect of MβCD on ATP depleted cells. (a) Averaged PSDs of cells (solid lines) and their backgrounds (dashed lines) in control, ATP dep. and ATP dep. + MβCD cells. (b) Single cell statistics of parameters of temporal fluctuations in these conditions. N = 10 cells each. (c) Single FBR statistics of temporal fluctuations parameters in the three mentioned conditions. $n_{control}$ = 333 FBRs, $n_{ATPdep.}$ = 235 FBRs, $n_{ATPdep.+MβCD}$ = 250 FBRs, N = 10 cells each. (d) Single cell statistics (top, N = 10 cells each) and single FBR statistics (bottom, $n_{control}$ = 333 FBRs, $n_{ATPdep.}$ = 235 FBRs, $n_{ATPdep.+MβCD}$ = 229 FBRs, N = 10 cells each) of SD_{space} in all three conditions. (e) Box plots of A, $η_{eff}$ and γ for single cell statistics. N = 10 each. (f) Single FBR statistics of the mechanical parameters in the three conditions. $n_{control}$ = 305 FBRs,

$n_{ATPdep.}$ = 207 FBRs, $n_{ATPdep.+M\beta CD}$ = 229 FBRs, N = 10 cells each. * p value < 0.05, ** p value < 0.001, ns p value > 0.05, Mann-Whitney U test. See **Table S4** for statistics.
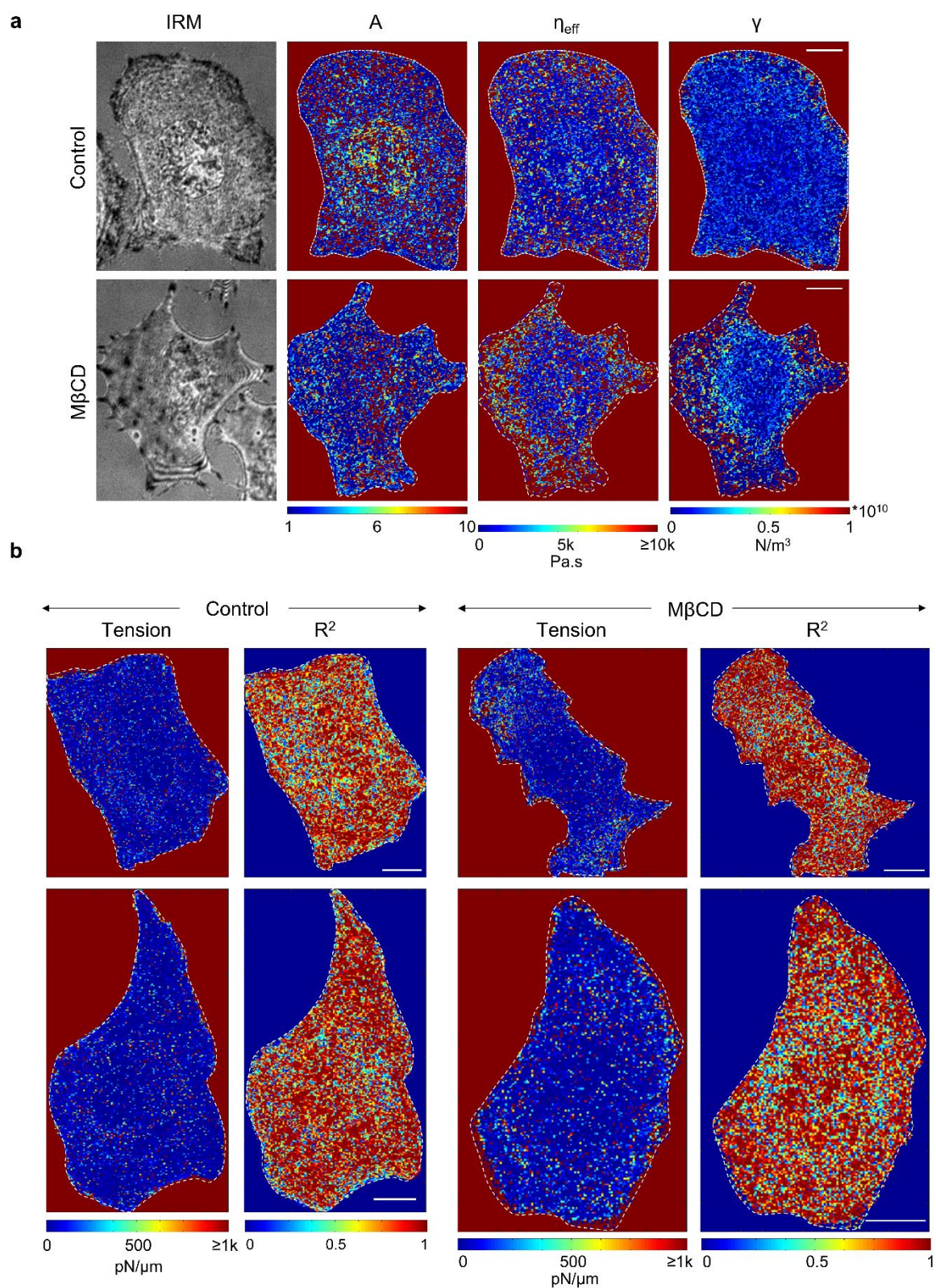
Figure S4

Figure S4: Maps of mechanical parameters on MβCD treatment. (a) Representative IRM images with single pixel maps of active temperature, cytoplasmic viscosity and confinement of a control and MβCD treated cell (tension map in Fig. 4e). Scale bar, 10 μm. The white dashed

lines mark the cell boundary. Fitting was performed for pixels inside this boundary. (b) Two representative single pixel maps of tension and R^2 for control and cholesterol depleted cells. Scale bar, 10 μm. The white dashed lines mark the cell boundary. Fitting was performed for pixels inside this boundary.
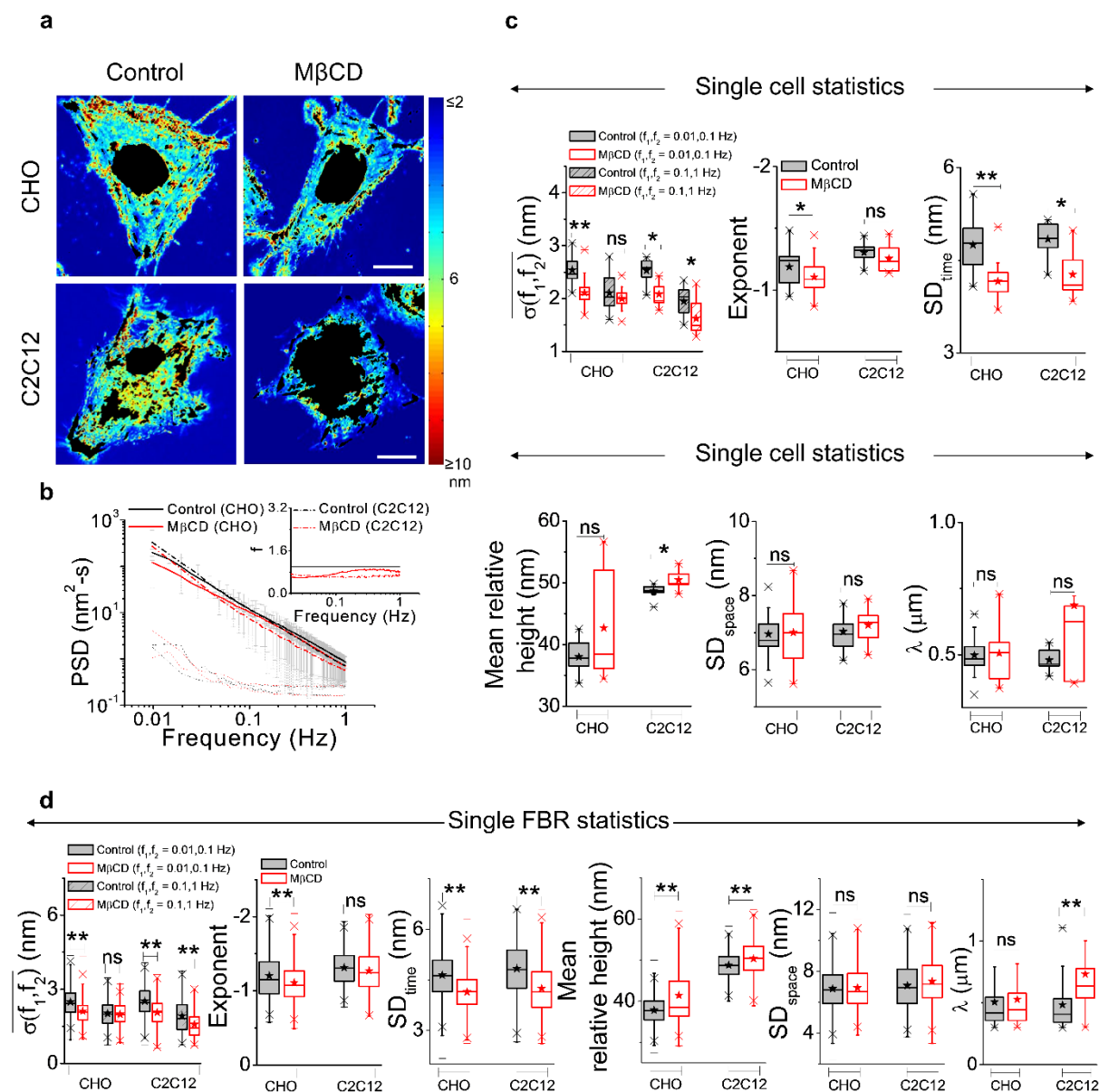
Figure S5

Figure S5: Effect of MβCD on detailed parameters of membrane fluctuations in different cell lines. (a) Representative whole cell SD_{time} maps of control vs. MβCD treated CHO (top, scale bar: 10 µm) and C2C12 (bottom, scale bar: 5 µm) cells. Non-FBRs are blackened out. (b) Averaged PSDs of CHO (solid lines) and C2C12 (dashed lines) cells in control and cholesterol depleted conditions with their respective backgrounds (dash and dotted lines); inset shows the ratio of the background subtracted PSDs of the two cell lines. (c) Box plots of single cell statistics for the parameters of temporal fluctuations and spatial undulations in both conditions for the two cell lines. N = 30 cells each in CHO, 10 cell each in C2C12. (d) Box plots of single FBR statistics for the parameters of temporal fluctuations and spatial undulations in both conditions for the two cell lines. $n_{CHO\ control}$ = 612 FBRs, $n_{CHO\ MβCD}$ = 369 FBRs, N = 30 cells each; $n_{C2C12\ control}$ = 219 FBRs, $n_{C2C12\ MβCD}$ = 179 FBRs, N = 10 cells each). * p value < 0.05, ** p value < 0.001, ns p value > 0.05, Mann-Whitney U test. See **Table S4** for statistics.
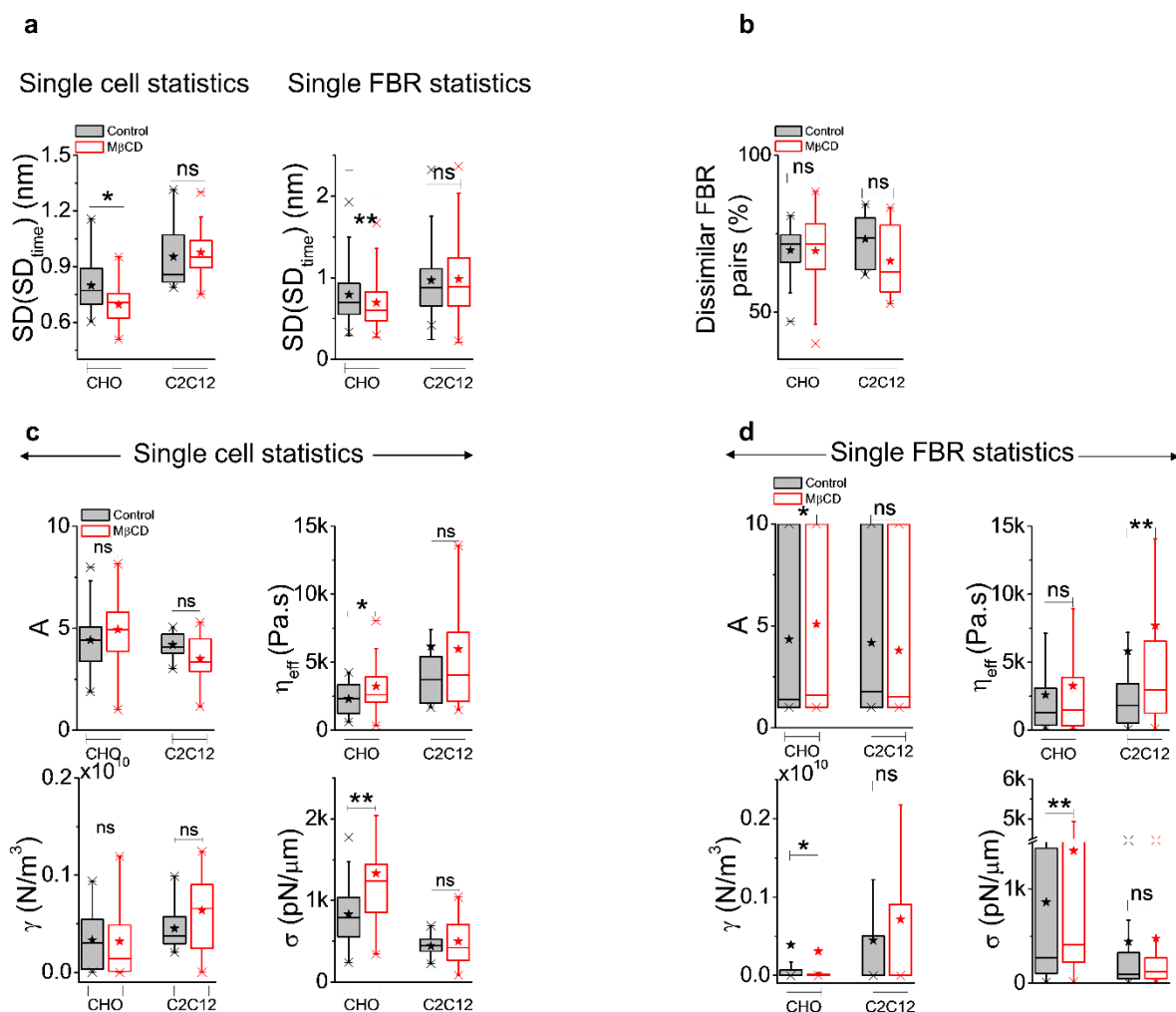
Figure S6

Figure S6: Effect of MβCD on fluctuations heterogeneity and mechanics in different cell lines. (a) A measure of intra-FBR fluctuations heterogeneity, $SD(SD_{time})$ in control and MβCD treated CHO and C2C12 cells in single cell statistics (left, N = 30 cell each for CHO, 10 cells each for C2C12) and single FBR statistics (right, $n_{CHO\ control}$ = 612 FBRs, $n_{CHO\ MβCD}$ = 369 FBRs, N = 30 cells each; $n_{C2C12\ control}$ = 219 FBRs, $n_{C2C12\ MβCD}$ = 179 FBRs, N = 10 cells each). (b) Intracellular long-range heterogeneity (dissimilar FBR pairs) in CHO (N = 30 cells each) and C2C12 cells (N = 10 cells each). (c) Membrane mechanical parameters A, η_{eff}, γ and σ obtained from fitting PSDs in CHO (N = 30 cells each) and C2C12 cells (N = 10 cells each) in control and cholesterol depletion. (d) Single FBR statistics of the mechanical parameters under the two conditions in the two cell lines. $n_{CHO\ control}$ = 495 FBRs, $n_{CHO\ MβCD}$ = 257 FBRs, N = 30 cells each; $n_{C2C12\ control}$ = 174 FBRs, $n_{C2C12\ MβCD}$ = 124 FBRs, N = 10 cells each. * p value < 0.05, ** p value < 0.001, ns p value > 0.05, Mann-Whitney U test. See **Table S4** for statistics.
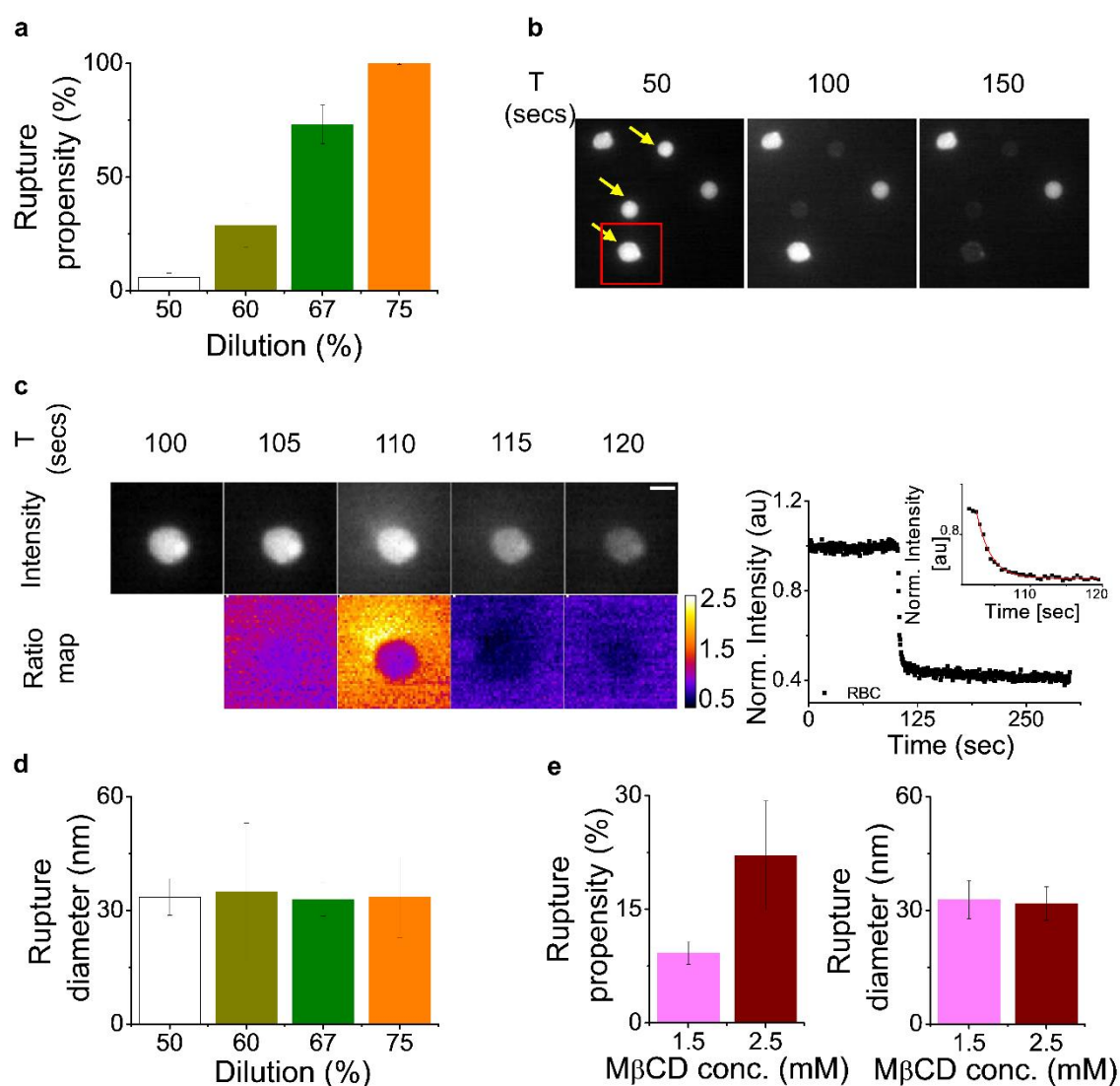
Figure S7

Figure S7: Rupture characteristics of RBCs. (a) Rupture propensity of RBCs with increase in osmotic stress. (b) Time lapse images of Calcein AM loaded RBCs undergoing rupture (arrows in yellow). (c) Intensity (top) and ratio map (bottom) of a rupturing RBC marked in (b) followed in time shows single point rupture. Right: A time profile of normalized mean intensity of a ruptured RBC; inset shows the double exponential fit to the profile. (d) Rupture diameter in RBCs with change in osmotic stress. (e) Rupture propensity (left) and rupture diameter (right) of RBCs treated with increasing concentrations of MβCD without hypo-osmotic shock administration. Mean ± SD of at least two experiments is plotted in each set. See **Table S4** for statistics.
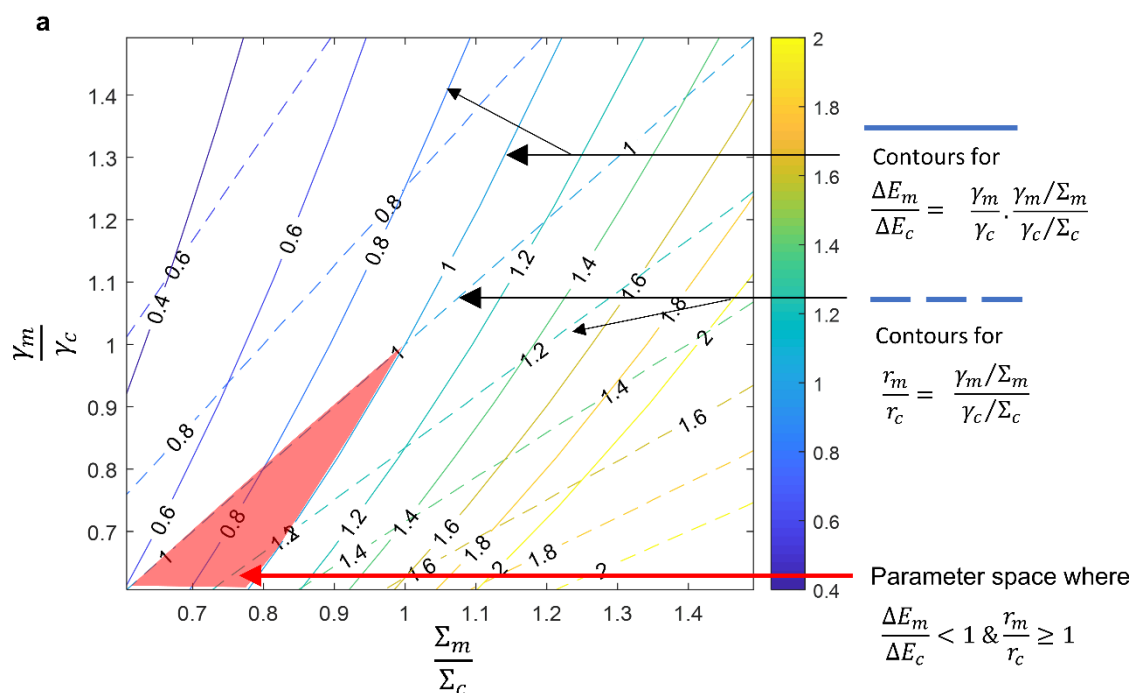
Figure S8

Figure S8: Lowered lysis surface and line tension on MβCD treatment. Contour plots of dependence of ratio of rupture radius of MβCD with control ($\frac{r_m}{r_c}$) & ratio of ΔE of MβCD with control ($\frac{\Delta E_m}{\Delta E_c}$) on the ratio of lysis surface tension between MβCD and control conditions ($\frac{\Sigma_m}{\Sigma_c}$) and on ratio of line tension between MβCD and control conditions ($\frac{\gamma_m}{\gamma_c}$). Contour lines closest to 1 are used to roughly map out the region in the parameter space where the observation of increased rupture propensity of ΔE ratio <1 and unchanged or increased rupture size ratio r ≥ 1 is true. Note that in this region both lysis surface tension ratio and line tension ratio (MβCD to control) is < 1, indicating lowered lysis surface and line tension on MβCD.
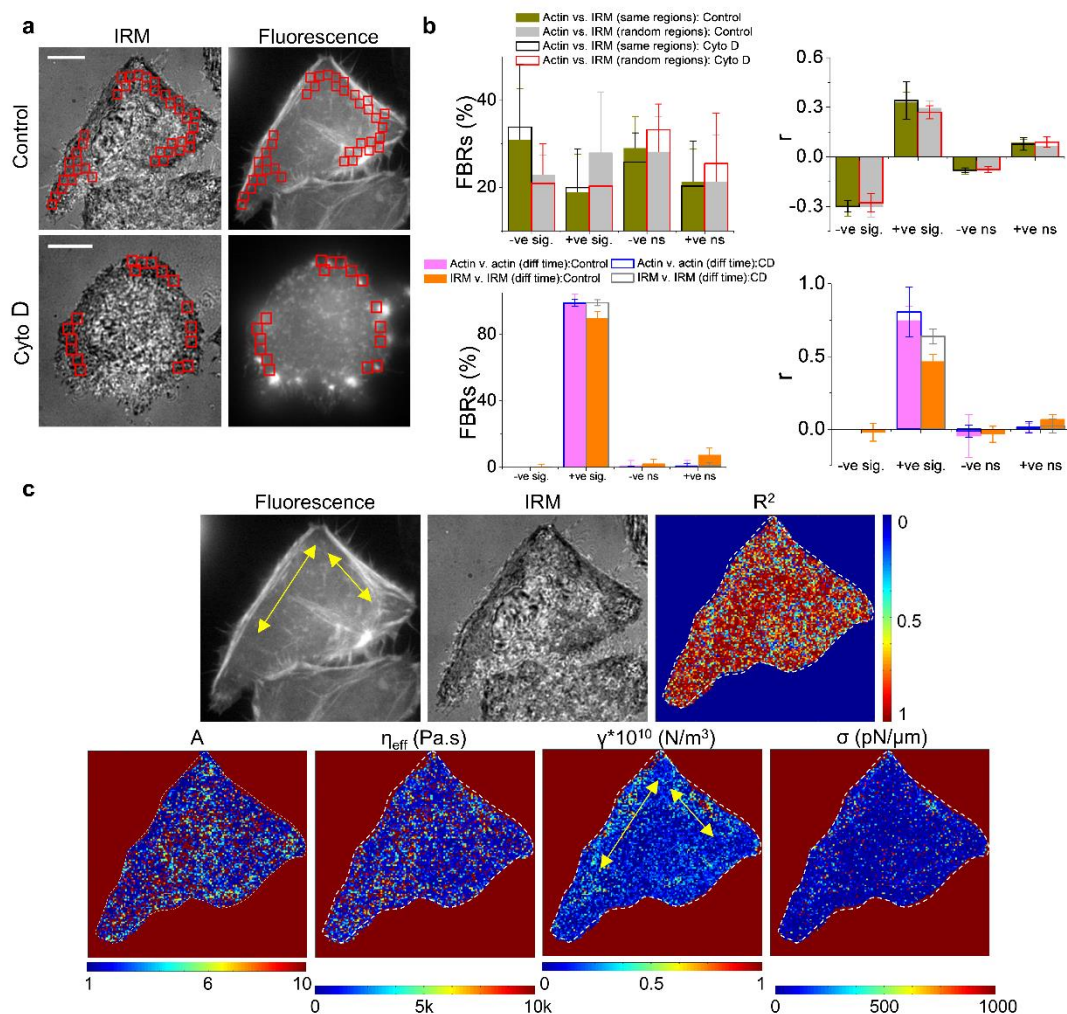
Figure S9

Figure S9: Actin density does not strongly affect IRM intensity at FBRs. (a) IRM and epifluorescence images of mEmerald-Lifeact-7 transfected control (top) and Cyto D treated (bottom) HeLa cells. Scale bar, 5 μm. (b) Top: plots of no of FBRs that show positive/negative correlation in actin and IRM intensities of same and random FBRs in control and Cyto D treated cells with their corresponding average Pearson correlation coefficients (r). Bottom: plots of no of FBRs that show positive/negative correlation in actin vs. actin and IRM vs. IRM intensities of same FBRs in and Cyto D treated cells with their corresponding average Pearson correlation coefficients (r). (c) Clockwise from top left: Fluorescence and IRM image of a control transfected cell, with its corresponding single pixel R^2, σ, γ, η_{eff} and A maps. The white dashed line marks the boundary of the cell. The yellow arrows mark the areas in confinement maps that faintly show the presence of stress fibres. Scale bar, 10 μm.
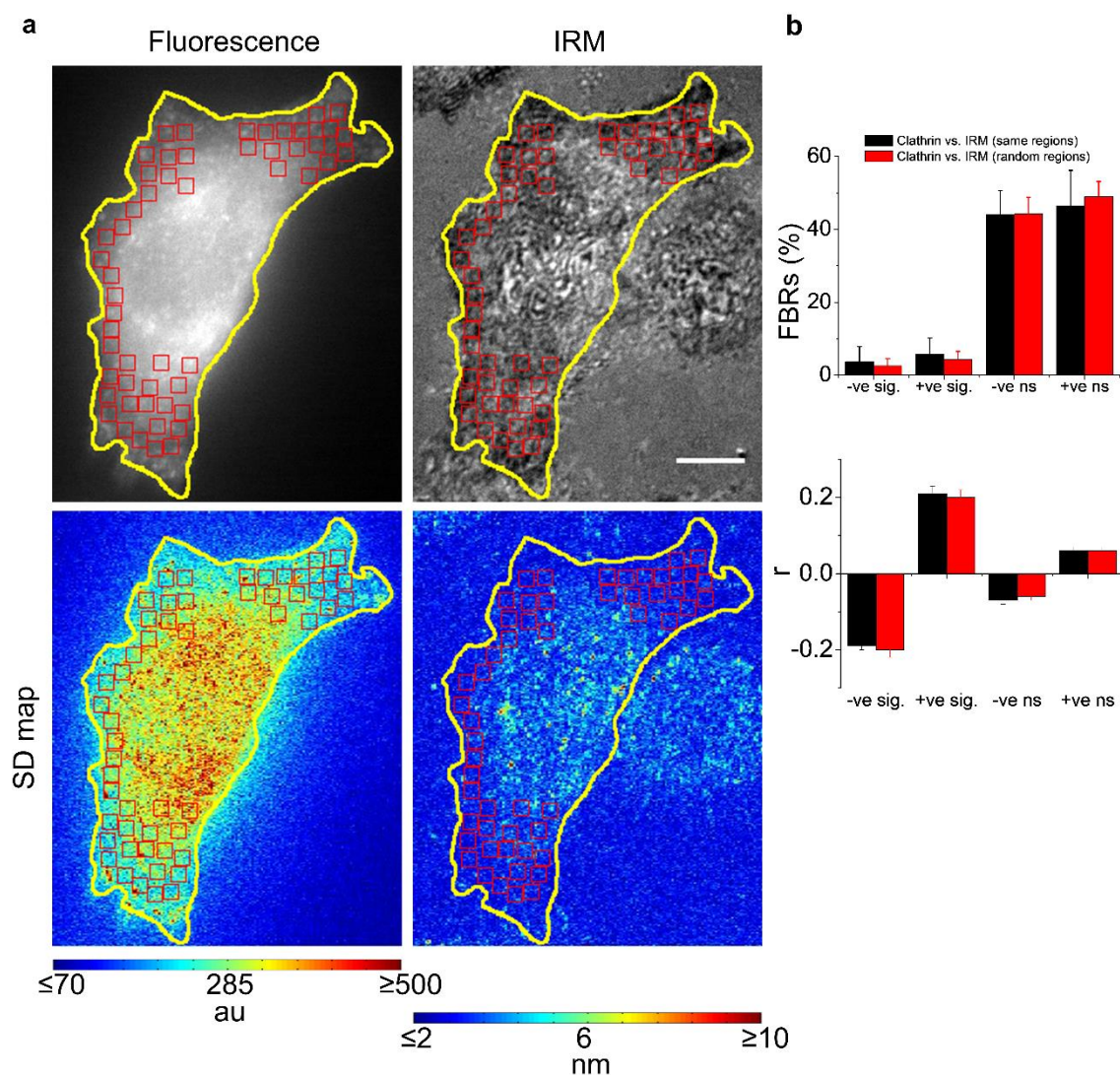
Figure S10

Figure S10: Mobile clathrin pits do not strongly affect IRM intensity fluctuations at FBRs. (a) Epi-fluorescence and IRM (top) images of mCherry-Clathrin LC-15 transfected control HeLa cells, with their corresponding SD maps (bottom). The boundary of the cell is marked in yellow. Scale bar, 10 μm. (b) Plots of no of FBRs that show positive/negative correlation in clathrin and IRM intensity fluctuations of same and random FBRs in cells (top) with their corresponding average Pearson correlation coefficients (r, bottom).

Supplementary Discussion

As elaborated in the reference (13), the energy needed to form a circular pore in the lipid bilayer can be written in terms of the line tension (γ), surface tension (Σ) and the radius of the pore (r):

$$E(r) = 2\pi r\gamma - \pi r^2 \Sigma$$

The surface tension at the time of rupture can be termed as lysis tension.

Minimizing energy ($\frac{dE}{dr} = 0$), yields $r = \frac{\gamma}{\Sigma}$ $\qquad$ (1)

The energy required to cross this critical radius r can be written as: $\Delta E = \frac{\pi\gamma^2}{\Sigma}$ $\qquad$ (2)

In this study, we have two conditions where control is denoted as 'c' and MβCD treatment is denoted 'm'. From experiments, we see that MβCD treatment increases propensity (Fig. S6e). Since the propensity, or probability to rupture in isotonic conditions is expected to be related thus: $P \propto e^{\frac{-\Delta E}{k_B T}}$, this implies

$$\frac{\Delta E_m}{\Delta E_c} < 1 \qquad \text{or,} \qquad \frac{\gamma_m^2/\Sigma_m}{\gamma_c^2/\Sigma_c} < 1 \qquad \text{or,} \qquad \frac{\gamma_m}{\gamma_c} \cdot \frac{\gamma_m/\Sigma_m}{\gamma_c/\Sigma_c} < 1 \qquad (3)$$

But, we also know that rupture diameter is unaltered on MβCD treatment (Fig. S6d)

$$\frac{r_m}{r_c} = 1 \qquad \text{or,} \qquad \frac{\gamma_m/\Sigma_m}{\gamma_c/\Sigma_c} = 1 \qquad (4)$$

From Eq. 3 and 4, it is evident that:

$$\frac{\gamma_m}{\gamma_c} < 1 \qquad (5)$$

This information, together with Eq. 4 implies that $\frac{\Sigma_m}{\Sigma_c} < 1$

or, that the lysis tension of MβCD treated cells needs to be lower than that of control cells.

Observations of increased rupture diameter ($\frac{r_m}{r_c} > 1$) on MβCD treatment (Fig. 4 e) in hypotonic condition are in line with this inference since enhanced propensity would still need the line tension and hence lysis tension to be lowered by MβCD treatment.

Table S3: Statistical parameters for data presented in main figures.

This is provided as a separate Excel sheet

Table S4: Statistical parameters for data presented in supplementary figures.

This is provided as a separate Excel sheet

Supplementary Movies

Movie S1: Time-lapse imaging of single HeLa cells under control and MβCD treated conditions at 37 ºC under IRM mode.

The movie shows the time evolution of the interference pattern of the basal membrane of single HeLa cells in control (left) and MβCD treated (right) condition. Scale bar: 10 µm. Stacks of 2048 images are captured at 19.91 frames/sec.

Movie S2: Time-lapse imaging of control and MβCD treated HeLa cells after administration of 95% hypo-osmotic shock at 37 ºC.

The movie shows the time evolution of the fluorescence of Calcein AM loaded HeLa cells under control (left) and with MβCD (right), after the application of a 95% hypo-osmotic shock. Scale bar: 100 µm. Images are captured every 2 secs for 5 mins.

Movie S3: Time-lapse imaging of RBCs before and after administration of 67% hypo-osmotic shock at 37 ºC.

The movie shows the time evolution of the fluorescence of Calcein AM loaded RBCs before (left) and after (right) the application of a 67% hypo-osmotic shock. Scale bar: 100 µm. Images are captured every 0.5 secs for 5 mins.

Movie S4: Time-lapse imaging of MβCD treated RBCs without the administration of 67% hypo-osmotic shock at 37 ºC.

The movie shows the time evolution of the fluorescence of Calcein AM loaded RBCs that are treated with 1.5 mM (left) and 2.5 mM (right) MβCD without the application of a 67% hypo-osmotic shock. Scale bar: 100 µm. Images are captured every 0.5 secs for 5 mins.

Supplementary References

1. Gov, N., A.G. Zilman, and S. Safran. 2003. Cytoskeleton confinement and tension of red blood cell membranes. Phys. Rev. Lett. 90: 228101.

2. Thoumine, O., O. Cardoso, and J.-J. Meister. 1999. Changes in the mechanical properties of fibroblasts during spreading: a micromanipulation study. Eur Biophys J. 28: 222–234.

3. Kim, T., M.L. Gardel, and E. Munro. 2014. Determinants of Fluidlike Behavior and Effective Viscosity in Cross-Linked Actin Networks. Biophys. J. 106: 526–534.

4. Joanny, J., and J. Prost. 2009. Active gels as a description of the actin-myosin cytoskeleton. HFSR J. 3: 94–104.

5. Betz, T., M. Lenz, J.-F. Joanny, and C.C. Sykes. 2009. ATP-dependent mechanics of red blood cells. PNAS. 106: 15320–15325.

6. Peukes, J., and T. Betz. 2014. Direct Measurement of the Cortical Tension during the Growth of Membrane Blebs. Biophys. J. 107: 1810–1820.

7. Alert, R., J. Casademunt, J. Brugués, and P. Sens. 2015. Model for Probing Membrane-Cortex Adhesion by Micropipette Aspiration and Fluctuation Spectroscopy. Biophys. J. 108: 1878–1886.

8. Simunovic, M., and G.A. Voth. 2015. Membrane tension controls the assembly of curvature-generating proteins. Nat. Commun. 6: 1–8.

9. Curie, M., S. Bernard, and P. Cedex. 2008. 3D Processing and Analysis with ImageJ e. Microscopy. Vi: 1–6.

10. Sens, P., and J. Plastino. 2015. Membrane tension and cytoskeleton organization in cell motility. J. Phys. Condens. Matter. 27: 273103.

11. Lieber, A.D., S. Yehudai-Resheff, E.L. Barnhart, J.A. Theriot, and K. Keren. 2013. Membrane Tension in Rapidly Moving Cells Is Determined by Cytoskeletal Forces. Curr. Biol. 23: 1409–1417.

12. Betz, T., and C. Sykes. 2012. Time resolved membrane fluctuation spectroscopy. Soft Matter. 8: 5317.

13. Moroz, J.D., and P. Nelson. 1997. Dynamically Stabilized Pores in Bilayer Membranes. Biophys. J. 72: 2211–2216.